Accepted version of IEEE-copyrighted article. The original version of this article is available at: https://ieeexplore.ieee.org/document/8932532.
DOI: 10.1109/JESTPE.2019.2959649

Pre-Emphasis Control in Switched-Mode Power Converter for Energy-Efficient Wide Bandwidth Visible Light Communication

L. Teixeira, F. Loose, J. M. Alonso, R. C. Beltrame,
C. H. Barriquello, V. Alfonso Reguera, and M. A. Dalla Costa

***Abstract*—Visible Light Communication (VLC) shows up as a trend for short-range wireless networks. However, from the energy point-of-view, there is still a lack of LED drivers that support considerable data rates with high efficiency. Common solutions would include Switched Mode Power Converters (SMPC), which are efficient, but they still face challenges regarding the modulation bandwidth for VLC. Thus, this paper presents an analysis of a Pre-Emphasis (PE) technique to overcome the low bandwidth constraint of SMPC. The PE filter is used to render the frequency response of the circuit to provide a wider bandwidth for communications. It operates on the duty cycle of the converter and it dictates the average output signal value over a switching period. Finally, the technique is presented in a theoretical approach with aligned experimental results in a 21.5 W buck-converter-based LED driver switched at 1 MHz, with 89% efficiency and an increased modulation bandwidth from 8.12 kHz to 450 kHz (55 times).**

Keywords*—*Visible Light Communication, VLC, LED Drivers, Efficiency, Pre-Emphasis.

I. Introduction

Visible light communication (VLC) enables a wide range of applications demanding data communication from Internet of Things connected devices [1], indoor localization, up to 5G mobile network attocells [2], among many others. As an extra feature, VLC demands that illumination infrastructure would also perform instantaneous light modulation, being performed at frequencies imperceptible to the human eye.

Although very promising, the realization of VLC modulation capable devices faces technical challenges concerning the bandwidth (BW) of light modulation [3]–[5], drop of efficacy of the LED [6], [7] and also electronic driver limitations [8], [9]. In order to not cause a substantial decrease in the energy efficiency of an illumination device, VLC needs to be seen as an incremental feature that is subject to several restrictions. Thus, the most energy-efficient approach is to use the well-known high efficient LED driver circuit topologies. Some workaround can be implemented to overcome their limitations on implementing light modulation.

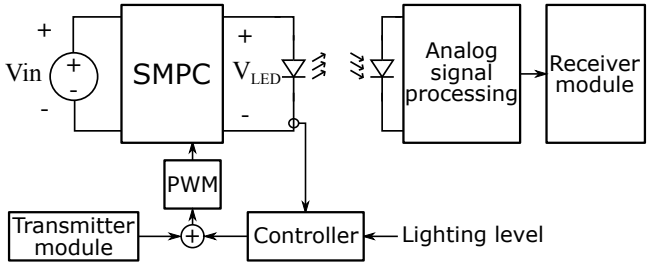

Fig. 1: Application of a SMPC as VLC LED driver.

Consumer electronic LED drivers are mostly designed using Switched Mode Power Converters (SMPC). They are more efficient power sources which also present reduced circuit volume, weight and cost due to the available range of switching frequencies of their semiconductors (hundreds of kHz to dozens of MHz). For VLC, those circuits may be used as modulators at the transmitter, as showed in [10]–[13]. One example of application and block diagram of a SMPC-based VLC system is depicted in Fig. 1. This diagram shows how the communication and lighting control are connected in a single VLC LED driver used to send data from transmitter to receiver modules. However, in terms of signal dynamics at the light output, single SMPCs [8], [10]–[13] are not the fastest drivers among other solutions reported for VLC. Therefore, in order to increase the system modulation bandwidth, some solutions have been proposed in the literature [14]–[17]. Nevertheless, these solutions require extra elements as linear amplifiers [14], [15] or extra switch modulators [16], [17], which penalize the efficiency and increase circuit complexity. An alternative solu-

tion that does not require extra power components is based on using the SMPC residual ripple to convey the information [10], [11], [13], which limits the system bandwidth due to the narrow converter filter cut-off frequency. Given these reasons, this work is focused on average current control, not on ripple modulation, since it enables the system to implement baseband and passband VLC modulation schemes.

We explore a method known as pre-emphasis (PE) or pre-equalization that was already applied to VLC to increase linear drivers BW [3]–[5]. Since then, available literature was focused on compensating the LED dynamic behavior. Hence, when applied to SMPCs, this strategy is effective to increase the modulation bandwidth with small gain and phase errors in the bandwidth of the interest [18], which is a novelty in the design of VLC lighting systems.

This work is organized as follows. Section II presents the control structure with PE of an LED driver. Section III presents an analysis of the SMPC with PE along with design considerations. Section IV presents simulation results confirming the model and analysis. Follows, Section V presents experimental results as well as performance metrics. Finally, Section VI summarizes the conclusions of our work.

II. Pre-emphasis Control of a VLC SMPC

First, this section presents the full control structure of a power converter with VLC. Second, the PE filter is contextualized in this system to provide background to the following method.

A. LED driver control scheme including PE

In LED lighting, control is mandatory to regulate the dc output current for illumination. It can be actively performed in a closed-loop scheme tracking a provided reference (I_{REF}). Fig. 2a presents the block diagram of a VLC LED driver as the schematic shown in Fig. 1 with additional PE filter. Fig. 2b shows the control diagram of a VLC LED driver with PE in the feedforward path. The controller $C_{AVG}(s)$ regulates a dc reference on the output (I_{LED}), and it operates on a bandwidth well below the one required for the VLC signal. Hence, the system transfer function (TF) from I_{REF} to I_{LED} is depicted in (1).

$$\frac{I_{LED}(s)}{I_{REF}(s)} = \frac{C_{AVG}(s)\,G_C(s)\,G_{LED}(s)}{1 + C_{AVG}(s)\,G_C(s)\,G_{LED}(s)} \qquad (1)$$

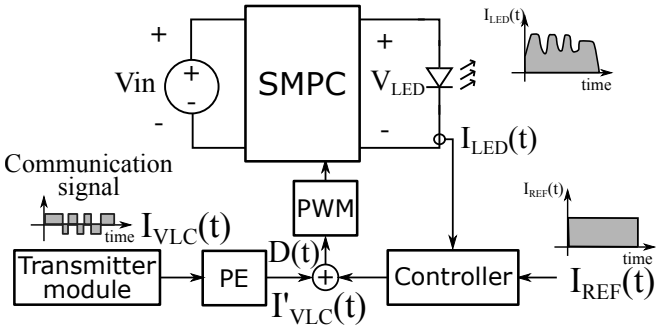

(a) System block diagram including PE.

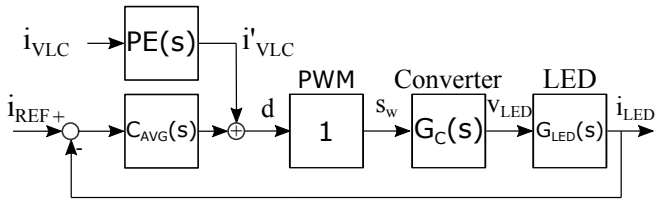

(b) Control diagram of a VLC LED driver with PE in the feedforward path.

Fig. 2: Representations of VLC LED driver with PE.

For good average light control, the gain of $C_{AVG}(s)$ must be high. This can be accomplished at low frequencies (near dc), so that $|C_{AVG}(s)G_C(s)G_{LED}(s)| >> 1$ and, in this case, $|I_{LED}(s)/I_{REF}(s)| \approx 1$, ensuring good average reference tracking.

Regarding the PE method, it compensates for the low-pass dynamics of the converter by inserting the data signal in a feedforward path on the driver control loop. Additionally, we may design the transfer function $PE(s)$ to overcome the low-pass characteristics of the plant seen by the communication signal. Thus, one way to analyze $PE(s)$ is by observing the transfer function that relates the data signal $I_{VLC}(s)$ to $I_{LED}(s)$, shown in (2).

$$\frac{I_{LED}(s)}{I_{VLC}(s)} = \frac{PE(s)\,G_C(s)\,G_{LED}(s)}{1 + C_{AVG}(s)\,G_C(s)\,G_{LED}(s)} \qquad (2)$$

The analysis of (2) is performed considering separated frequency ranges. The first range is for average current control for lighting (near dc). The second concerns communication signal band (higher frequencies). In the lower band, $C_{AVG}(s)$ has a high gain ($|C_{AVG}(s)G_C(s)G_{LED}(s)| >> 1$), thus rendering $I_{LED}(s)/I_{VLC}(s) \approx PE(s)/C_{AVG}(s)$, showing that the controller will reject any communication signal in this band. Moreover, in the communication signal band, the average controller $C_{AVG}(s)$ does not actuates if its gain is low in such frequency. Thus

$|C_{AVG}(s)G_C(s)G_{LED}(s)| << 1$ and, in this case, $I_{LED}(s)/I_{VLC}(s) \approx PE(s)G_C(s)G_{LED}(s)$. Finally, this last is the TF that is used to design the PE filter.

In this work, we addressed the digital control design based on a DSP. This structure allows for a lower sampling rate of I_{LED}, since the bandwidth of the control loop is much lower than the bandwidth of the signal for communication (BWS). Attention is required to provide a suitable anti-aliasing filter according to the signal sampling frequency. Thus, the computation of $C_{AVG}(s)$ can also be performed in a slower pace. Only the PE filter and the PWM modulator are required to operate at the switching frequency rate.

B. *Pre-emphasis filter*

Starting from the known distortion that the duty cycle (D) signal suffers when passing through the SMPC circuit, according to TF in (2), an inverse effect can be applied to I_{VLC} stimuli to give the complete system response a constant gain and linear phase in the interest band. Some assumptions, the conditions to apply this method and consequences to the system dynamics are further explored next.

In commercial LED drivers, the filter is the main dynamic limiting factor one would find to modulate light for VLC. In SMPC LED drivers operating with a switching frequency below 1 MHz, the bandwidth of the filter (BWF), bandwidth of G_C in Fig. 2b, is usually designed below 100 kHz, in order to limit the high frequency output current ripple. In this case, the intrinsic cutoff frequency of phosphor-covered LEDs, which is usually around 3 MHz, represents a secondary factor that does not limit the modulation bandwidth. Therefore, the PE method is used to cope with the frequencies in the range between BWF and $F_S/2$.

The PE filter can be implemented in a continuous- or discrete-time domain, and it shall be integrated to the converter into the $D(t)$ value provided to the PWM modulator. Thus, the amplitude drop at the passive filter output will be compensated by the PE filter. The frequency response of this filter is depicted in the Bode diagram of Fig. 3. It shows a small magnitude drop as well as little distortion into the signal phase within the additional bandwidth that can be occupied by VLC signal using PE. Although it seems a narrow band of spectrum in Fig. 3, this additional bandwidth corresponds to 80% of

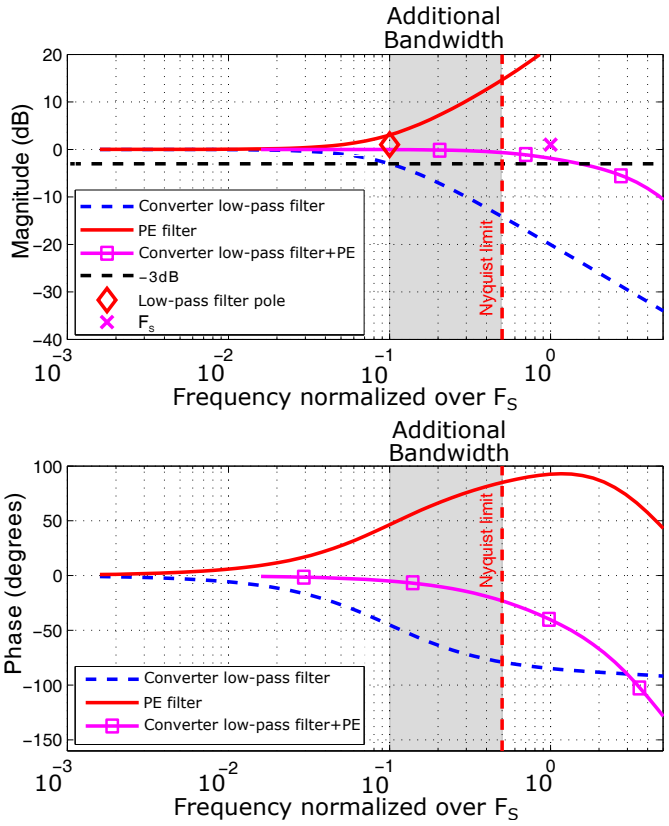

Fig. 3: Frequency response of the system parts and its expected converter with PE behavior.

the useful bandwidth below the limit imposed by Nyquist criterion.

III. Details of PE implementation to VLC SMPC

In order to provide context, firstly we present a generic structure and model of a SMPC. Secondly, the basis and limitations of the PE method are explored. Finally, we present the design of the average controller and PE filter.

A. *Generic model of SMPCs*

In VLC applications and LED lighting, the most common SMPC encountered are derived from the principles of the step-down buck converter. These SMPC circuits are responsible for filtering a digitally pulsed signal generated by the PWM in order to obtain its average value, depending on the inductance (L) and capacitance (C) of the filter.

The switching frequency F_S directly affects the filter BW, while dc regulation is expected for average illumination level. Therefore, Fig. 4 presents a generalization of the power structure of a SMPC, in

which the main converter power blocks are: switch arrangements and passive filter. For better visual perception the frequency of pulses in S is lower than the necessary to produce v_{LED} as smooth as shown in the figure. The switches provide a PWM voltage. The average gain over a switching period is then defined by $D(t)$, which is the main control variable and responsible to transfer data to the output current and also regulate the dc light level.

The method explored in this work allows the generation of any signal shape for VLC that may be accomplished in baseband by controlling changes of $D(t)$ over time. However, the limitations to the average current control method are the switching frequency and the dynamics given by the frequency response of the passive elements and the LED load. First, F_S dictates the pace of the PWM, and it limits the changes of $D(t)$ by one switching period to another. Second, the BWF, which plays a major role on the output dynamic, may distort the signal in the case when BWS>BWF, if not properly compensated.

Therefore, we may represent the signal path for communications and lighting by the open-loop TF block diagram of Fig. 4. A PWM with pulses aligned at the beginning of the period behaves similarly to a zero-order hold and, therefore, it causes no significant distortion to the signal in the band of interest that comes from dc to F_S/2. A linear phase lag is caused in the signal band indeed, however it represents a constant time delay. Therefore, a constant gain was adopted for the PWM frequency response in this analysis.

The converter TF $G(S) = \hat{V}_{LED}(s)/\hat{S}(s)$ represents a filter dynamic for perturbations around the operating point. The output voltage frequency components that can be controlled by $D(t)$ are within the limits of zero and $F_S/2$, due to the Nyquist criterion imposed by the PWM. For example, Fig. 4 depicts the case in which the signal (D) occupies a bandwidth that slightly exceeds BWF, hence most of the energy outside this range is lost, stored in the passive elements, leading to a smooth signal shape in v_{LED}. Without any additional signal processing stage, if the BWS is wider than the BWF, the communication signal degrades its shape, affecting the communication capabilities.

B. Current residual ripple as a design constraint

The residual ripple cannot be avoided in the converter output, that is presented in Fig. 4 by

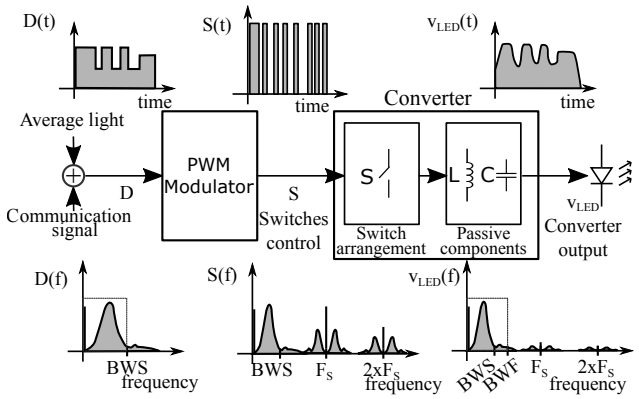

Fig. 4: Expected signal measured at each stage when BWF > BWS.

V_{LED}, and corresponds to the frequency components around F_S and its harmonics. The choice of F_S/BWF ratio directly impacts ripple intensity in the converter output. In this sense, the higher the BWF, for the same F_S, the more ripple amplitude in the output.

Ripple percentage can be expressed by the ratio of ac rms value over average [7]. Alternatively, for pure sinusoidal ripple, it can be calculated as peak deviation over average [19]. A small ripple does not account for significant detriment in converter efficiency, nor in LED efficacy or visual perception, if F_S is allocated in a flicker-free band. However, more intense ripple may cause a drop in converter efficiency (due to higher component stress) and LED efficacy drop. As a reference, a small ripple factor of less than 20% applied to a power LED device causes an LED efficacy drop of less than 2% [7].

The LED linearized model is electrically represented by the threshold voltage (V_{th}) with the series LED dynamic resistance (R_{LED}) [19], which is valid while forward biased and around a given operating point. The current ripple factor (γ) can be calculated from the LED instantaneous current (i_{LED}) and average current (I_{LED}), as presented in (3).

$$\gamma = \frac{i^{AC}_{LED\_rms}}{I_{LED}} \tag{3}$$

where $i^{AC}_{LED\_rms}$ is the ac rms ripple of the LED current.

The frequency harmonic components of i_{LED} are directly defined by the filter bandwidth according to the ratio F_S/BWF. Fig. 5 presents an abacus for

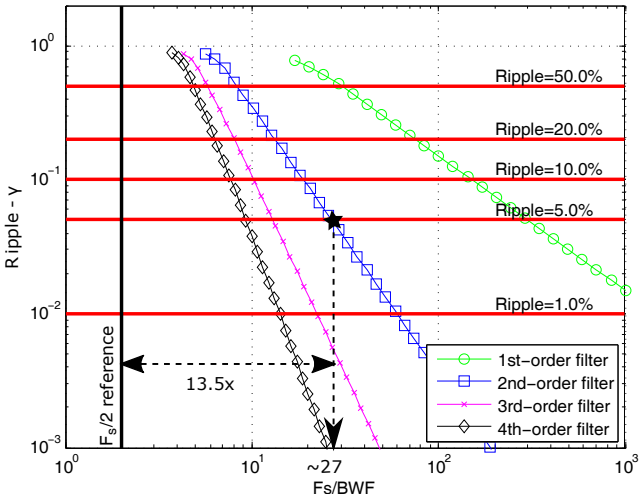

Fig. 5: Ripple factor abacus according to a range of F_S/BWS for filters up to 4^{th} order.

this relation for filter order up to 4 using commercial high power LED parameters [20] and D=0.5.

C. Foundation for PE method in SMPC

The application of the PE filter in SMPC PWM generation is possible due to the following identified opportunities:

1) Excess of control energy: It is available due to the converter TF and LED voltage to current reasonable gain, $G_{LED}(s) = 1/R_{LED}$, valid for perturbations at frequencies below 3 MHz in white LEDs. The fine control of the converter output during dc regulation generates regular small changes to $D(t)$. Therefore, there is still enough excursion on the control signal for intentional modulation. Hence, such facts allow the increase of signal power specially in components that are attenuated by the following stages of the converter.

2) The F_S/BWF ratio: It is limited in its minimum value by the ripple that is allowed by design, as explored in the previous section. In this sense, the less residual ripple that is allowed from the F_S/BWF ratio, the more room exists for acting with PE (see Fig. 3). As an example, a ripple level below 5% can be achieved using a second-order filter with minimum ratio of $F_S/\text{BWF} \approx 27$, as can be seen in the solid star marker in Fig. 5. That leaves room for a bandwidth increase of ≈ 13.5 times, in the F_S/BWF range from 27 to 2, as pointed by the dashed arrow in the figure.

These opportunities turned the application of the PE method possible, although the physical inertia of the filter is the key to understand why the components above BWF have a higher cost for intentional modulation. This and other limitations to the exposed method are explored in next section.

D. Limitations of PE method

There are two main identified aspects of the PE method that are disadvantages: i) dynamic range of I_{VLC} and ii) coupling between signal frequency components inside the bandwidth of interest and switching harmonic components outside of it. These aspects are addressed in the analysis that follows.

Inductor inertia is analyzed by the current rise and fall rates (dI_L/dt) or the slew-rate the system can perform. Hence, the inductance value (L) and the voltage applied (V_L) are the converter parameters that determine this performance, according to inductor branch equation $V_L = L\, dI_L/dt$. This example approaches an inductor, but a similar analysis is also valid for a capacitor or high order filters containing multiple reactive components.

Moreover, to generate any frequency component, modeled as a pure sinusoidal current signal $A\ sin(wt)$, its rise and fall rates are the main concern on regarding the system dynamic. They are dependent on the signal amplitude and frequency, in this case $d(A\ sin(wt))/dt = Aw\ cos(wt)$. As the $cos(wt)$ part is within the range $[-1, +1]$, to track it in the filter output the value of dI_L/dt shall match or exceed $[-Aw, +Aw]$. This analysis can be expanded to any signal that is the sum of several components, which leads to the conclusion that the higher frequencies require more rise and fall rates, thus having higher cost to be generated.

Given these facts, to generate a signal using limited rise and fall rates one can either reduce its bandwidth (decrease the w) or its amplitude (A). However. it is common that in SMPCs the V_L applied to the filter is different at each operating stages, leading to different rise and fall rates. This comes with filter requirements and it is not a design choice. Nevertheless, when it is modeled around an operating point and for small deviations in $D(t)$, the linear TF $G_C(s)$ is still valid.

Furthermore, not only the slew-rate shall be considered, but also the $D(t)$ dynamic range limits the PE method to avoid pronounced distortion to the

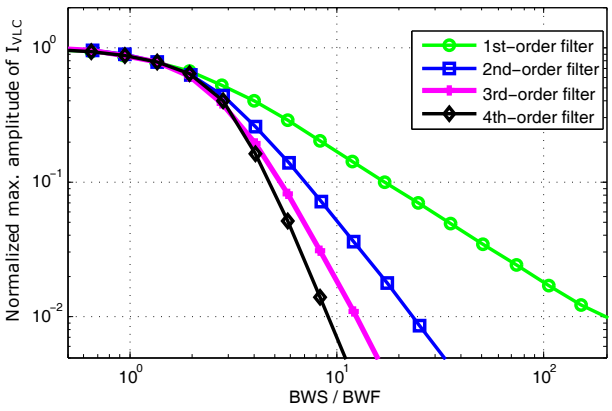

Fig. 6: Maximum amplitude of I_{VLC} according to the relationship of signal and filter bandwidths.

communication signal, $D(t) \in [0, 1]$. The duty cycle is generated by the addition of the control action from C_{AVG} and the VLC signal i'_{VLC}, as depicted in Fig. 2b. However, only the latter is considered in this analysis because the former is much slower than the communication signal, as explained in Section III-E. Thus, the BWS will impact directly in i'_{VLC}, which can be expressed as in (4).

$$\begin{aligned} i'_{VLC}(t) =& \mathcal{L}^{-1}\left(I_{VLC}(s) \cdot PE(s)\right) = \\ &\approx \sum_i \left(PE_i \cdot I_{VLCi}\, sin(w_i t + \phi_i)\right) \end{aligned} \tag{4}$$

where $\mathcal{L}^{-1}$ stands for inverse Laplace transformation, I_{VLCi}, w_i and ϕ_i are the amplitude, angular frequency and phase, respectively, of the signal harmonics, and PE_i is the PE filter gain for each harmonic.

There is no closed expression to calculate the signal excursion from (4). However, according to the central limit theorem, when the ac signal is composed of a great number of uncorrelated and random components inside a wide frequency band, e.g. an OFDM signal, it can be approximated in time domain by a normal distribution of zero mean value [21]. This can be easily proven by numeric simulations. According to this, if the BWS is increased beyond BWF, the PE method will increase the dynamic range of i'_{VLC}, even though the dynamic range of i_{VLC} is kept constant. This happens due to the PE higher gain in the signal path at frequencies attenuated by the converter, which is a clear limitation of this method.

In order to clarify the previous relations, numerical simulations were performed to obtain the maximum amplitude of i_{VLC} as a function of the ratio between BWS and BWF. In this sense, the maximum allowed amplitude of i_{VLC} is the one which assures that the duty cycle will be within its operating limits. The results are shown in Fig. 6 for different filter orders, where the maximum amplitude of i_{VLC} has been normalized with respect to its value at a very low BWS/BWF ratio. By respecting this maximum amplitude, no signal distortion will occur using the PE method, neither by high frequency attenuation, nor by signal clipping. Additionally, as can be seen in Fig. 6, there is a trade-off between amplitude and bandwidth increment: the higher the bandwidth, the lower the amplitude. Therefore, lower order filters are preferred to be used with PE method because the amplitude reduction is less intense than for higher order filters. For example, to generate a signal with 10 times bandwidth using PE, $\mathrm{BWS/BWF} = 10$, a first-order filter only reduces the signal amplitude 5.9 times, while second-, third- and forth-order filters reduce it 18.4, 54.3 and 141.3 times, respectively.

However, the limitation in the signal i_{VLC} excursion must not be considered a very negative aspect of this method when applied to VLC LED drivers. This is because small current excursions are expected in the LED, so that its efficacy is not very affected by the communication, as addressed in Section III-B.

Finally, the PE method presents an implicit coupling between harmonic components inside the bandwidth of interest and switching frequency sideband components. This comes from the fact that the PWM generation creates components in the bandwidth with respective and proportional replicas around switching frequency and its harmonics. Therefore, the increase in the useful signal intensity will also cause an increase in higher harmonic components at frequencies above half of switching frequency, which are not used for communication purposes. This unwanted harmonic content will be further attenuated by the filter indeed, however they increase components current stress and LED efficacy drop.

E. Design of average current controller

The average current controller $C_{AVG}(s)$ shall be specified to comply with the following two requirements: performing good reference current tracking against slow perturbations (with

$C_{AVG}(s)G_C(s)G_{LED}(s) >> 1$ at low frequencies) and having low gain ($C_{AVG}(s)G_C(s)G_{LED}(s) << 1$) in the VLC signal band to avoid rejecting these components. In this situation, the converter passive components dynamics ($G_C(s)$) have the dominant poles, therefore defining the system bandwidth. We suggest that the requirements can be accomplished with $C_{AVG}(s)$ as a low-pass filter (bandwidth < BWF) or an integrator, but keeping in mind that the gain and phase margin of direct path $C_{AVG}(s)G_C(s)G_{LED}(s)$ shall be taken into account for gain tuning.

F. Design of the PE filter

The PE filter can be designed following the steps:

1) determine the linear TF of the stages that need to be compensated as presented in (2);
2) determine poles and zeros of this TF using PE equal to 1;
3) the PE filter TF is designed using poles and zeros cancellation, which is a straightforward control strategy.

A generic model for a PE filter using poles and zeros cancellation is given in (5).

$$PE(s) = \frac{\prod_{i=1}^{N_p}(1 + s/w_{SPi})}{\prod_{i=1}^{N_z}(1 + s/w_{SZi}) \prod_{i=1}^{N_p - N_z}(1 + s/w_{PPi})} \tag{5}$$

in which w_{SPi} and w_{SZi} are poles and zeros angular frequencies of (2) when PE is made equal to 1. N_p and N_z are the number of poles an zeros, respectively. Also the product of $(1 + s/w_{PPi})$ ensures stability of the PE filter providing at least the same number of poles as the number of zeros [18]. However, it must be assured that when selecting w_{PPi} frequency, the system should not introduce any phase distortion, which can be achieved by ensuring that the phase of the system TF behaves linearly within the communication signal bandwidth. In this way, the received signal will only present a time delay, but no additional distortion.

In a well tuned implementation of this filter, accordingly to (5), the product of the PE TF with the compensated system will have a flat dynamic response up to $w_{PPi}\ rad/s$, thus rendering performance similar to the shown in Fig. 3.

IV. Simulation of linear system

Using the control structure described, the PE method was simulated using a model of a generic power converter. A mathematical software platform was used to simulate the system with ideal switches and a linear power filter. The filter of the power converter was designed to be of first order with no zeros and the switching frequency selected was 1 MHz. The ratio F_S/BWF was selected as 100, thus ensuring an output ripple of about 15% (see Fig. 5). The design of the PE filter was performed according to the converter TF and considering the procedure described in Section III-F. In this design example, the filter and converter TFs correspond to those in Fig. 3. The pole of the converter and the zero of the PE filter were located at the same frequency of 10 kHz. Also, the additional pole was added to the PE filter in order to assure its stability. Since the communication signal bandwidth goes from 10 kHz to 450 kHz, the pole was located at a frequency one decade beyond 450 kHz. The selected frequency was 5 MHz. This design method assures no phase distortion owing to the cancellation effect around 10 kHz and because the PE filter pole at 5 MHz has no effect on the communication signal.

The test communication signal extends from $0.01F_S$ to $0.45F_S$ with a flat power spectral density (PSD). It is adequate to depict the performance of the system and does not exceed the Nyquist limit in $0.5F_S$. A small band between the signal and $0.5F_S$ was intentionally left clear for better understanding and visual separation between the components of interest and the others in the spectrum. Moreover, that is the expected PSD of a wide-band multi-carrier scheme like an Orthogonal Frequency Division Multiplexing (OFDM) or a Discrete Multi Tone (DMT) using the whole available band. However, such approach is not restricted to those modulations, since it ensures that any scheme using this band will be generated without significant distortion.

The modulated pulse train, S_W in Fig. 2b, was applied to the linear system TF. In Fig. 7a, it is possible to verify that the output current has a pronounced residual ripple. Nevertheless, the filtered version of these signals, which keeps only the components below $0.5F_S$, shows a good reproduction of the original communication signal. It is easy to note that the simulation with PE strategy performs much better tracking of the VLC signal than the one

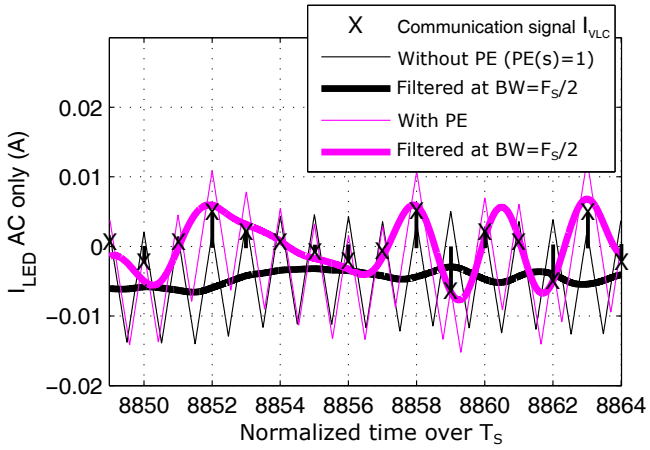

(a) Transient behavior of simulated PE.

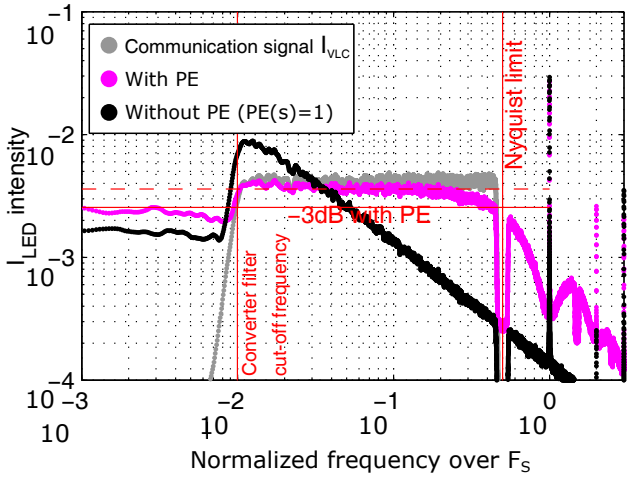

(b) Spectrum of simulated PE.

Fig. 7: Simulation results with and without PE strategy.

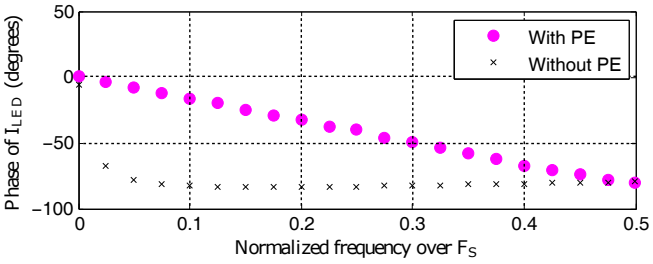

(a) Phase of simulated PE.

Fig. 8: Simulation results with and without PE strategy.

without it. That can be explained by the attenuation of a great part of the components and this effect is confirmed in the spectrum of I_{LED} shown in Fig. 7b. Additionally, Fig. 8a presents the linear phase lag using PE caused by a constant time delay, while without PE a clear phase distortion occurs. Moreover, comparing these simulated magnitude and phase results with the ones in the Bode diagram

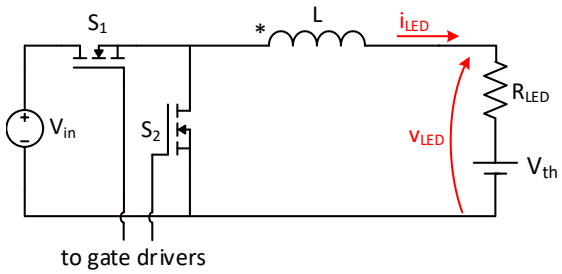

(a) Synchronous buck circuit.

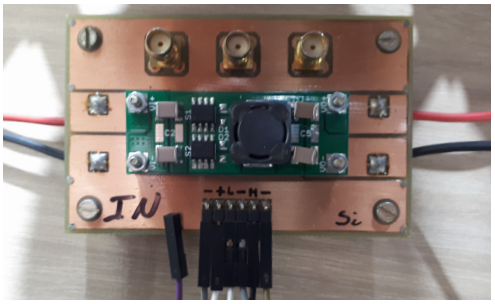

(b) Converter prototype.

Fig. 9: LED driver circuit used in the experimental test.

of the whole system in Fig. 3 confirms that behavior. After the compensation with PE, the frequency band occupied by the test signal resides inside the bandwidth of the system below a -3 dB cutoff.

V. Experimental Validation

For experimental validation of the PE technique, we used a synchronous buck SMPC driving a high power LED. The values of the parameters used in experimental validation are the same as in the simulation, with the exception of the converter filter cut-off frequency that was the closest possible with available components. The converter circuit, designed with a first order filter, is depicted in Fig. 9. This SMPC is commonly used for LED drivers due to its simplicity and good efficiency in applications that do not require electrical isolation.

The control structure was implemented using a digital signal processor (DSP), similar to the feed-forward VLC signal with PE, and the converter design ensures duty cycle around 0.5 for the expected average LED current ($\overline{I_{LED}}$). The experimental setup parameters and operating conditions are synthesized in Table I. The input voltage was defined accordingly to keep the converter operating at 0.5 duty cycle, which is the same simulated operating point. The first order filter BWF is 8.12 kHz, therefore $F_S/\mathrm{BWF} = 123$, that results in the

TABLE I: Experimental test setup parameters, components and results summary.

Parameter	Symbol	Value
Synchronous buck converter		
Switching frequency	F_S	1 MHz
Input voltage	V_{in}	63.2 V
Average output voltage	$\overline{V_o}$	28.5 V
Average output current	I_{LED}	0.75 A
Output power	P_o	21.5 W
Semiconductor switches	S_1, S_2	IRF7492
Semiconductor driver		MAX15019A
Digital Signal Processor		TIVA TM4C1294
Inductor	L	47 μH
Average duty cycle	$\overline{D}$	0.5
LED Bridgelux Vero 18 BXRC-50C4000-F-24 [20]		
Threshold voltage	V_{th}	26.8 V
Dynamic series resistance	R_{LED}	2.4 Ω
Average LED current	$\overline{I_{LED}}$	0.75 A
PE filter parameters in (5)		
PE filter zero frequency	w_{SP1}	8.12 kHz
System dynamic		
Original system bandwidth		8.12 kHz
Increased system bandwidth		450 kHz

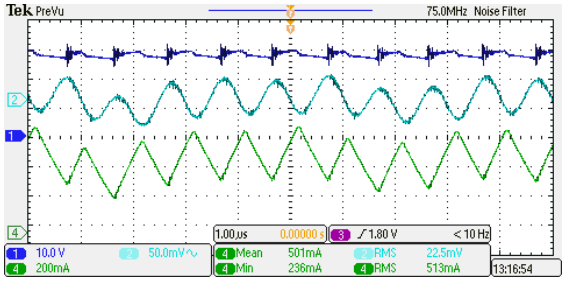

(a) From top to bottom: Detail of V_{LED} (ch. 1), captured light (ch. 2) and I_{LED} (ch. 4).

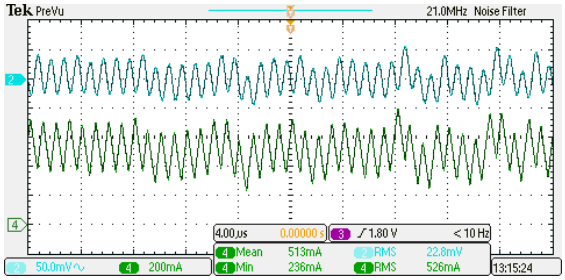

(b) From top to bottom: captured light signal (ch. 2) and view of the dynamic of I_{LED} (ch. 4).

Fig. 10: Measurement results on oscilloscope.

ripple factor of 18%, calculated considering (3) and without any intentional modulation. In fact, after intentional modulation, the current excursion was increased up to 24%, calculated following (3). In this case, all frequency components are accounted, which includes ripple and signal.

We captured the light using a light transducer (Vishay BPW34S light sensor with an analog signal amplifier, 1.1 MHz of bandwidth) at the distance of 2 m. From the performed experiments, it is possible to confirm the effectiveness of the PE and the prototype performance is presented on the following results. Firstly, the oscilloscope plot shown in Fig. 10 clearly depicts the dynamic in the LED current and the light captured. Observing either the time domain behavior (Fig. 11a) or its spectrum (Fig. 11b), it is possible to see that they match with the predicted behavior (Fig. 3) and the simulated spectrum (Fig. 8). Fig. 11c presents the phase lag of signal harmonic components which trends to a linear shift, the linear trend of the PE measurements is shown as a dashed line in this figure. Furthermore, comparing to the communication signal provided with the filtered I_{LED} in Fig. 11a, it is clear that with PE the current follows the expected shape; while without PE it is very degraded due to attenuated frequency components.

In the measurement of a 40,000 periods vector, it was verified 30.3 dB of signal-to-noise and distortion ratio between the received light and communication signal I_{VLC} at the transmitter. This comparison was performed in the signal bandwidth, in this case the signal processing performed in the receiver is responsible for ignoring ripple harmonic components above $F_S/2$ frequency. This evidence confirms the effectiveness of the explored technique for VLC. Moreover, it showed that no significant distortion occurred to the signal although it went through PWM modulator, power stage and LED.

Furthermore, the LED light signal was also captured. It was verified that it presents very similar time and spectrum behaviors as those shown for the LED current in Fig. 11. Only additional attenuation was verified for components that were above the light sensor bandwidth, which are out of the interest band. Fig. 12 presents operating efficiency measurements of the proof of concept converter according to the ripple factor resulting from different modulation intensities, that in this case indicates different communication signal power levels. In this figure, it is clear to see that the converter has same efficiency with or without PE applied to the stimulus when comparing the same output signal power level.

A. *Comparison*

Table II presents a comparison among the current work prototype and other published solutions using SMPC-based VLC LED drivers. The modulation factor is the ratio between standard deviation and average value of output current ($\sigma_{I_o}/\overline{I_o}$), and it is

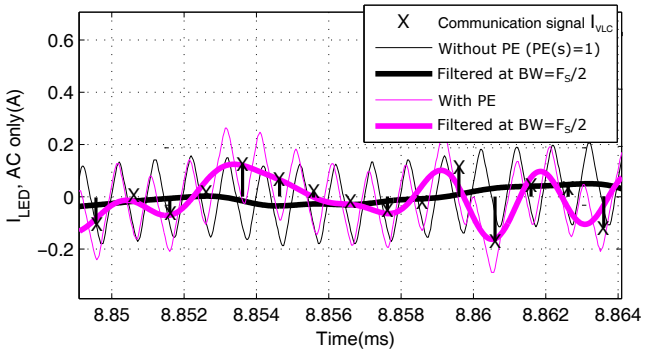

(a) Transient behavior of experimental PE test.

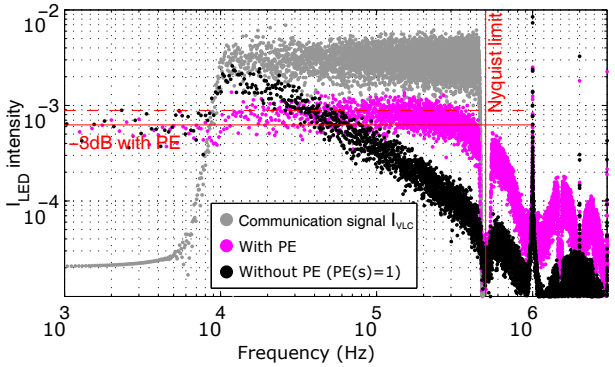

(b) Spectrum of experimental PE test.

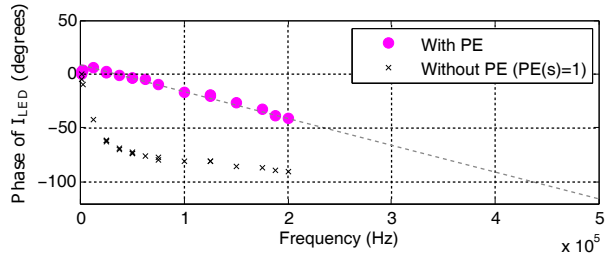

(c) Phase of experimental PE test.

Fig. 11: Measurement results with and without PE strategy.

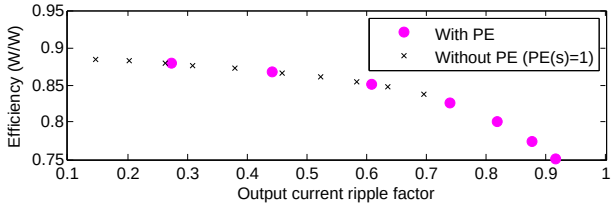

Fig. 12: Efficiency measurements according to the ripple factor.

used to compare the amplitude of modulated signals inside signal band. As can be seen, all solutions employ buck and buck-derived topologies to implement current modulation. The two-phase converters have effective double switching frequency when compared to single-phase ones. In this work, a ratio F_S/BWS of 2.2 has been achieved, which is the lowest one of the compared solutions using average current control. Therefore, considering the limitation imposed by F_S the signal bandwidth of this solution is among the highest in literature. Also solutions using ripple modulation have similar performance and achieve reasonable signal amplitude [10], [11], [13], see modulation factor in Table II.

VI. Conclusions

The foundations of PE technique were explored and its suitability to application in a SMPC for light modulation was explained. The analysis, simulation and experimental results showed that it performs as expected and can be implemented with no hardware changes to the power converter. It was demonstrated that the room for bandwidth improvement using this method is dependent on the switching frequency and converter filter design, thus it can be analysed with respect to the converter output ripple. Also, the analysis of the limits of this method showed that the increment in bandwidth and output communication signal excursion present a trade-off.

In the experimental test presented, without using any strategy as PE, the intentional modulation would have to be restricted on a bandwidth of about 1/123 of F_S (8.12 kHz) due to the allowed current ripple to avoid pronounced distortion. On the other hand, using the described PE strategy, in a, experimental proof of concept, the converter showed an increment of 55 times the original bandwidth.

Furthermore, we demonstrated from the analysis that using this strategy the signal bandwidth can reach up to $F_S/2$ without significant distortion or intersymbol interference. That represents a significant reduction, under equal output ripple restrictions, to the F_S needed to synthesize the same VLC signal. Therefore, the PE technique has shown to be an effective method to overcome the low bandwidth issues commonly encountered in VLC applications involving SMPC.

Acknowledgment

The experimental measurements would not be possible without the support provided by the colleges in GEDRE, special thanks to Renan Duarte, Christian Miguel Barth and João Paulo Sales Brum. This study was financed in part by the Coordenação de Aperfeiçoamento de Pessoal de Nível Superior - Brasil (CAPES) - Finance Code 001, PROEX

TABLE II: Comparison among VLC LED driver solutions using average and ripple modulation in SMPC.

Reference	Output power (W)	Mod. factor ($\sigma_{I_o}/\overline{I_o}$)	Efficiency (%)	F_S(MHz)	F_S/BWS	Modulator topology
[8][a]	6.7	0.28	90	5	4.15 (8.3 §)	Two-phase buck
[9][a]	1.7	1	85	0.10	10	Buck
[12][a]	10.1	0.28	91.3	10	3.44 (6.9 §)	Two-phase buck [d]
[22][a]	4.3	0.64	81	10	10	Buck
[23][a]	1	-	63	0.10	10	Buck
[24][a]	97.98	0.4	92	10	3.2 (6.4 §)	Two-phase buck
[10][b]	22.6	0.29	91	0.1	2	Synchronous buck
[11][b]	10	0.44	86	0.5	3 (6 §)	Two-phase synchronous buck
[13][b]	10	0.5	96.5	0.5	8.33 (16.7 §)	Two-phase synchronous buck
This work[a]	21.5	0.1	89	1	2.2	Synchronous buck

[a] Uses average modulation. F_S/BWS is calculated from 0 up to signal bandwidth in baseband. Ripple components exist out of signal band.
[b] Uses ripple modulation. F_S/BWS is calculated using the signal bandwidth around switching carrier frequency, thus in passband.
[c] In parenthesis, it is F_S/BWS calculated using effective F_S, two-phase converters have doubled F_S with regard to the switching frequency of a single switch.
[d] Additional single-phase synchronous buck converter is used to process dc voltage.

program, PRPGP/UFSM, INCT-GD, CAPES proc 23038.000776/2017-54, CNPq proc 465640/2014-1, FAPERGS proc 17/2551-0000517-1.

Complementary media

Detailed description of experiment and media that do not fit the main paper length and proposal is presented in *this online presentation (web link)*. URL: https://gitlab.com/sr-lucasteixeira/pe-control-in-smpc-for-energy-eff-wide-bw-vlc. Additional media file is a complementary material and it is not meant to replace the original paper content.

References

[1] I. Demirkol, D. Camps-Mur, J. Paradells, M. Combalia, W. Popoola, and H. Haas, "Powering the Internet of Things Through Light Communication," IEEE Communications Magazine, vol. PP, pp. 1–7, 2019.

[2] H. Ma, A. Mostafa, L. Lampe, and S. Hranilovic, "Coordinated Beamforming for Downlink Visible Light Communication Networks," IEEE Transactions on Communications, vol. 66, no. 8, pp. 3571–3582, 2018.

[3] N. Fujimoto and H. Mochizuki, "477 Mbit/s visible light transmission based on OOK-NRZ modulation using a single commercially available visible LED and a practical LED driver with a pre-emphasis circuit," Optical Fiber Communication Conference and Exposition and the National Fiber Optic Engineers Conference (OFC/NFOEC), 2013, pp. 1–3, 2013.

[4] F. M. Wu, C. T. Lin, C. C. Wei, C. W. Chen, Z. Y. Chen, H. T. Huang, and S. Chi, "Performance comparison of OFDM signal and CAP signal over high capacity RGB-LED-based WDM visible light communication," IEEE Photonics Journal, vol. 5, no. 4, 2013.

[5] H. Li, X. Chen, J. Guo, Z. Gao, and H. Chen, "An analog modulator for 460 MB/S visible light data transmission based on OOK-NRS modulation," IEEE Wireless Communications, vol. 22, no. 2, pp. 68–73, 2015.

[6] A. Tsiatmas, F. M. J. Willems, J. P. M. G. Linnartz, S. Baggen, and J. W. M. Bergmans, "Joint illumination and visible-Light Communication systems: Data rates and extra power consumption," 2015 IEEE International Conference on Communication Workshop, ICCW 2015, pp. 1380–1386, 2015.

[7] L. Teixeira, F. Loose, J. P. Brum, C. H. Barriquello, V. A. Reguera, and M. A. Dalla Costa, "On the LED Illumination and Communication Design Space for Visible Light Communication," IEEE Transactions on Industry Applications, vol. 55, no. 3, pp. 3264–3273, 2019.

[8] J. Sebastian, D. G. Lamar, D. G. Aller, J. Rodriguez, and P. F. Miaja, "On the Role of Power Electronics in Visible Light Communication," IEEE Journal of Emerging and Selected Topics in Power Electronics, vol. 6, no. 3, pp. 1210–1223, sep 2018.

[9] X. Deng, Y. Wu, K. Arulandu, G. Zhou, and J.-p. M. G. Linnartz, "Performance Analysis for Joint Illumination and Visible Light Communication using Buck Driver," IEEE Transactions on Communications, vol. 66, no. 5, pp. 2065–2078, 2018.

[10] F. Loose, L. Teixeira, R. R. Duarte, M. A. Dala Costa, C. H. Barriquello, M. A. Costa, and C. H. Barriquello, "On the Use of the Intrinsic Ripple of a Buck Converter for Visible Light Communication in LED Drivers," IEEE Journal of Emerging and Selected Topics in Power Electronics, vol. 6, no. 3, pp. 1235–1245, 2018.

[11] J. Rodriguez, D. G. Lamar, P. F. Miaja, and J. Sebastian, "Reproducing Single-Carrier Digital Modulation Schemes for VLC by Controlling the First Switching Harmonic of the DC-DC Power Converter Output Voltage Ripple," IEEE Transactions on Power Electronics, vol. 33, no. 9, pp. 7994–8010, 2018.

[12] J. Rodríguez, D. G. Lamar, P. F. Miaja, D. G. Aller, and J. Sebastián, "Power Efficient VLC Transmitter Based on Pulse-Width Modulated DC-DC Converters and the Split of the Power," IEEE Transactions on Power Electronics, vol. 34, no. 2, pp. 1726 – 1743, 2019.

[13] J. Rodriguez, D. G. Lamar, D. G. Aller, P. F. Miaja, and J. Sebastian, "Reproducing Multi-Carrier Modulation Schemes for Visible Light Communication with the Ripple Modulation Technique," IEEE Transactions on Industrial Electronics, no. Early access, 2019.

[14] J. Kosman, O. Almer, A. V. N. Jalajakumari, S. Videv, and H. Haas, "60 Mb / s , 2 meters Visible Light Communications in 1 klx Ambient using an Unlensed CMOS SPAD Receiver," Photonics Society Summer Topical Meeting Series (SUM), 2016 IEEE, vol. 1, pp. 171–172, 2016.

[15] Z.-Y. Wu, Y.-L. Gao, J.-S. Wang, X.-Y. Liu, and J. Wang, "A Linear Current Driver for Efficient Illuminations and Visible Light Communications," Journal of Lightwave Technology, vol. 36, no. 18, pp. 3959–3969, 2018.

[16] K. Modepalli and L. Parsa, "Lighting Up with a Dual-

Purpose Driver," 2 IEEE Industry Applications Magazine, no. March/April, pp. 2–12, 2017.

[17] M. L. G. Salmento, G. M. Soares, J. M. Alonso, and H. A. C. Braga, "A Dimmable Off-line LED Driver with OOK-M-FSK Modulation for VLC Applications," IEEE Transactions on Industrial Electronics, vol. 0046, no. c, pp. 1–1, 2018.

[18] A. G. Tormo, "Bandwidth extension techniques for high-efficiency power amplifiers," Ph.D. dissertation, Technical University of Catalunya, 2011. [Online]. Available: http://upcommons.upc.edu/handle/10803/22706

[19] P. S. Almeida, V. C. Bender, H. A. Braga, M. A. Dalla Costa, T. B. Marchesan, and J. M. Alonso, "Static and dynamic photoelectrothermal modeling of LED lamps including low-frequency current ripple effects," IEEE Transactions on Power Electronics, vol. 30, no. 7, pp. 3841–3851, 2015.

[20] Bridgelux, "Bridgelux Vero 18 array series," Bridgelux, Tech. Rep., 2013. [Online]. Available: https://www.bridgelux.com/resources/ds32-bridgelux-vero-18-data-sheet-gen-6

[21] B. P. Lathi, Modern Digital and Analog Communications Systems, 3rd ed., A. S. Sedra and M. R. Lightner, Eds. Nova York: Oxford University Press, 1998.

[22] C.-S. A. Gong, Y.-C. Lee, J.-L. Lai, C.-H. Yu, L. R. Huang, and C.-Y. Yang, "The High-efficiency LED Driver for Visible Light Communication Applications," Scientific Reports, vol. 6, no. 1, p. 30991, 2016.

[23] X. Deng, Y. Wu, K. Arulandu, G. Zhou, and J.-p. M. G. Linnartz, "Performance comparison for illumination and visible light communication system using buck converters," 2014 IEEE Globecom Workshops (GC Wkshps), pp. 547–552, 2014.

[24] J. Sebastián, P. Fernández-Miaja, F. J. Ortega-González, M. Patiño, and M. Rodríguez, "Design of a Two-Phase Buck Converter With Fourth-Order Output Filter for Envelope Amplifiers of Limited Bandwidth," Transactions on Power Electronics, vol. 29, no. 11, pp. 5933–5948, 2014.

Lucas Teixeira (S'11) was born in Venâncio Aires, Brazil, in 1989. He received the B.S. degree in Electrical Engineering in 2012 and M.Sc. degree in Computer Science in 2015, both from the Federal University of Santa Maria (UFSM), Brazil. He is currently working towards the PhD degree in electrical engineering. His research interests include light-emitting-diode lighting systems, internet of things and visible light communication systems.

Felipe Loose (S'17) was born in Cruz Alta, Brazil, in 1991. He received his B.S. and M.Sc. degrees in electrical engineering by the UFSM in 2016 and 2018, respectively. He is currently pursuing his Doctoral degree at the same institution. His research interests include power electronics applications, solid-state lighting systems, digital signal processing and visible light communications.

J. Marcos Alonso (S'94, M'98, SM'03) received the M. Sc. Degree and Ph. D. both in electrical engineering from the University of Oviedo (UniOvi), Spain, in 1990 and 1994 respectively. Since 2007, he is a full Professor of the Electrical Engineering Department of the UniOvi. His research interests include lighting applications, dc-dc converters, power factor correction, resonant inverters, and power electronics in general.

Rafael Concatto Beltrame (S'10–M'13) was born in Santa Maria, Brazil, in 1984. He received the B.S., M.S., and Ph.D. degrees in electrical engineering from the Federal University of Santa Maria (UFSM), Santa Maria, Brazil, in 2008, 2009 and 2012, respectively. His research interests include high-performance power converters for renewable energy sources, design of gate-driver circuits for power electronics and tests of electric power transformers.

Carlos Henrique Barriquello was born in Três Passos, RS, Brazil, in 1984. He received the B.Sc., M.Sc. and Ph.D. degrees in Electrical Engineering from the UFSM in 2007, 2009 and 2012, respectively. His research interests include embedded and real time systems, wireless sensor and actuator networks, lighting systems, visible light communications and smart grid communication networks.

Vitalio Alfonso Reguera received the B. Eng. degree in telecommunications and electronics engineering from the Universidad Central "Marta Abreu" de Las Villas (UCLV), Cuba. He received the M.Sc. degree in telecommunications engineering, and the Ph.D. degree in electrical engineering from the same university in 2000 and 2007, respectively. His current research interests include wireless networks, communication protocols and IoT.

Marco Antônio Dalla Costa (S'03, M'09, SM'17) was born in Santa Maria, Brazil, in 1978. He received the B.S. and M.Sc. degrees in Electrical Engineering from the UFSM, Brazil, in 2002 and 2004, respectively. His research interests include dc/dc converters, power factor correction, lighting systems, high-frequency electronic ballasts, light-emitting-diode systems, renewable energy systems, solid state transformers, and visible light communication systems.